Communications in Nonlinear Science and Numerical Simulation 117 (2023) 106906

Contents lists available at ScienceDirect

Communications in Nonlinear Science and Numerical Simulation

journal homepage: www.elsevier.com/locate/cnsns

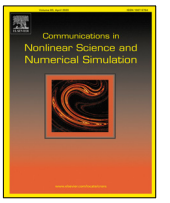

Research paper

Non-extensive entropy and fragment–asperity interaction model for earthquakes

A. Posadas [a,b,*,1], O. Sotolongo-Costa [c,1]

[a] Departamento de Química y Física, Universidad de Almeria, 04120 Almeria, Spain
[b] Instituto Andaluz de Geofísica, Campus Universitario de Cartuja, Universidad de Granada, 18071 Granada, Spain
[c] Cátedra de Sistemas Complejos "Henri Poincaré", Universidad de La Habana, Habana, 10400, Cuba

ARTICLE INFO

Article history:
Received 15 June 2022
Received in revised form 14 September 2022
Accepted 23 September 2022
Available online 29 September 2022

Keywords:
Fragment–asperity interaction model
Non-extensive entropy
Earthquake

ABSTRACT

In this study, we developed a fragment–asperity interaction model for earthquakes. Based on Tsallis entropy, this model can provide mathematical expression for the non-extensive entropy of fragments and asperities in the gouge area. From a statistical physics perspective, we hypothesized that non-extensive entropy decreases with energy relaxation after crustal rupture (i.e., following an earthquake). By using a windowing process, the non-extensive entropy value was monitored for three relatively recent earthquakes: the 2009 M6.1 L'Aquila (Italy) earthquake, 2011 M9.0 Tohoku (Japan) megathrust earthquake, and 2016 M7.8 Kaikoura (New Zealand) earthquake. The results support our hypothesis and suggest that the non-extensive entropy formula obtained in this study can provide a good characterization of seismicity for a given area.

© 2022 The Author(s). Published by Elsevier B.V. This is an open access article under the CC BY-NC-ND license (http://creativecommons.org/licenses/by-nc-nd/4.0/).

1. Introduction

The second law of thermodynamics postulates that only those phenomena for which the entropy of the universe increases, understood as a Shannon's measure of information [1], are allowed. Thus, in the field of seismology, entropy can be used to ascertain the future states of a given region of Earth's crust from its current state [2]. Changes in entropy have been identified as precursors of large earthquakes [3]. Entropy based in Boltzmann–Gibbs statistical physics can correctly describe Markovian processes, including complex systems exhibiting short-range correlations in space and time and short memory [4]. In contrast, systems displaying non-Markovian processes, including long-range correlations in space and time, long memory, and multifractal geometry (e.g., earthquakes), can be better described through non-extensive statistical physics; that is, they can be more appropriately characterized using Tsallis entropy [5].

From the point of view of statistical mechanics, entropy measures the number of microstates that can form a given state. Then, isolated systems tend to evolve to those states that can be formed by more microstates; that is, to the most probable [6,7].

Sarlis et al. [8] showed that the entropy of seismicity in natural time under time reversal changed sharply 2 months before the 2011 M9 Tohoku (Japan) earthquake. Moreover, by using a complexity measure that quantifies the entropy change of seismicity under time reversal, Varotsos et al. [9] found that a M7.3 earthquake on 9 March 2011 was a foreshock of the Tohoku mainshock.

* Corresponding author at: Departamento de Química y Física, Universidad de Almeria, 04120 Almeria, Spain.
E-mail address: aposadas@ual.es (A. Posadas).

[1] All authors contributed equally to the design of the methodology, discussion, analysis and revisions of the manuscript.

https://doi.org/10.1016/j.cnsns.2022.106906
1007-5704/© 2022 The Author(s). Published by Elsevier B.V. This is an open access article under the CC BY-NC-ND license (http://creativecommons.org/licenses/by-nc-nd/4.0/).

As far as Tsallis entropy is concerned, Telesca [10] analysed spatial variation of the non-extensive parameter q in Italy using a $1^\circ \times 1^\circ$ spatial window and suggested that different earthquake triggering mechanisms govern seismicity; that is, stick–slip when q is relatively low and fragment–asperity interaction when q is relatively high. The same author showed that volcano seismicity is characterized by relatively low q values [11], and that the non-extensive parameter q increased in the seismic interval before the 2009 M6.1 L'Aquila earthquake [12]. Valverde-Esparza et al. [13] indicated a possible correlation between the non-extensive parameter q and the seismicity pattern associated with subduction inclination angle. Michas et al. [14] used non-extensive physics to investigate the statistical properties of frequency–magnitude and interevent time distributions in the western Corinth Rift. Papadakis et al. [15] identified an increase in q before the 1995 M7.2 Kobe earthquake, indicating the system's transition away from equilibrium in preparation for energy release. Varotsos et al. [16] analysed the entropy change of seismicity under time reversal before the 2011 M9.0 Tohoku earthquake. Moreover, Skordas et al. [17] found that, just before the Tohoku earthquake, the Tsallis entropic index q of non-extensive statistical mechanics started to show distinct changes. In summary, the non-extensive entropic index q exhibits a precursory increase before large earthquakes [9].

2. Entropy

The main aim of statistical physics is to describe the macroscopic behaviour of complex systems from their microscopic properties. Boltzmann showed that entropy could be used to connect microscopic motions of particles to the macroscopic world; in his analysis, entropy is proportional to the number of accessible micro-states of the system (Ω) and it is expressed by the Boltzmann equation:

$$S = k\ ln\ \Omega \tag{1}$$

where k is Boltzmann's constant. Gibbs [18] generalized Boltzmann's entropy for systems described by other macroscopic variables as:

$$S = -k \sum_{i=1}^{\Omega} p_i \log\ p_i \tag{2}$$

where p_i is the probability of the system being in the ith state. The concept of entropy was later incorporated into information theory by Shannon [19] and Shannon and Weaver [20] as a measure for uncertainty. They defined the Shannon entropy $H(p)$ as the negative information measure; that is:

$$H\ (p) = -I\ (p) = -\sum_{i=1}^{W} p_i \log\ p_i \tag{3}$$

where $H(p)$ is always positive or zero. Shannon entropy is noted with the symbol H instead of S since it is a measure of information [1] or the lack of information.

Tsallis [21] introduced a generalization of classical statistical mechanics, termed non-extensive statistical mechanics, to better describe complex systems. Usually, complex systems exhibit power law distributions between some of their variables, fractal or multifractal geometries, and long-range interactions [4]. As such, non-extensive statistical mechanics offers an ideal framework to describe seismic phenomenon, and has given rise to a scientific field known as non-extensive statistical seismology [22]. While classical statistical mechanics is based on Boltzmann–Gibbs entropy, non-extensive statistical mechanics is based on Tsallis entropy. Tsallis [23] outlined various disadvantages of Boltzmann–Gibbs entropy and proposed the definition of non-extensive entropy as:

$$S = \frac{k}{q-1}\left(1 - \sum_{i=1}^{W} p_i^q\right) \tag{4}$$

where q is a real number called the entropic index. The standard distribution that characterizes Boltzmann–Gibbs statistics is a particular case of Tsallis entropy with a limit of q = 1. The main difference between classical and Tsallis entropies is that while the former is an extensive property of the system, the latter is non-extensive [22]. This means that if A and B are two probabilistically independent systems (i.e., $p_{ij}^{A+B} = p_i^A \cdot p_j^B$), for every ith and jth states, then Boltzmann–Gibbs entropy satisfies:

$$H\ (A+B) = H\ (A) + H(B) \tag{5}$$

while Tsallis entropy satisfies:

$$\frac{S(A+B)}{k} = \frac{S(A)}{k} + \frac{S(B)}{k} + (1-q)\,\frac{S(A)}{k}\frac{S(B)}{k} \tag{6}$$

Eq. (6) is the fundamental principle of non-extensive statistical mechanics [4] and the concepts of superextensivity, extensivity, and subextensivity correspond to $q < 1$, $q = 1$, and $q > 1$, respectively.

In this context, an earthquake is considered a critical phenomenon in a complex system that experiences a phase transition; several physical models have been developed to describe their essential properties [24]. Thereby, the maximum entropy principle has widely been applied in many out-of-equilibrium systems in physics (and other sciences), providing novel insights into their macroscopic states [4]. Berrill and Davis [25], Shen and Manshina [26], and Main and Burton [27] pioneered the use of the maximum entropy principle to explain distributions of earthquake magnitude and seismic energy release.

3. Fragment–asperity model

Sotolongo-Costa and Posadas [28] introduced the fragment–asperity interaction model for earthquake dynamics based on the non-extensive statistical formalism; in this model, the released seismic energy ε is related to the size of the fragments that fill the space between fault blocks. Silva et al. [29] slightly revised the fragment–asperity model using a volumetric relationship between seismic energy and fragment size instead of a linear one, in accordance with the standard theory of seismic moment scaling with rupture length [30]. Subsequently, Darooneh and Mehri [31] and Telesca [32,33] further refined the fragment–asperity model by introducing a function between earthquake magnitude and relative energy released as follows [34]:

$$M \propto \frac{2}{3}\log(\varepsilon) \tag{7}$$

According to these studies, if $N(>M)$ is the cumulative distribution of the number of earthquakes N with magnitude greater than M, then:

$$\frac{N(>M)}{N} = \left[\frac{1-\left(\frac{1-q}{2-q}\right)\left(\frac{10^{M}}{a^{2/3}}\right)}{1-\left(\frac{1-q}{2-q}\right)\left(\frac{10^{M_0}}{a^{2/3}}\right)}\right]^{\frac{2-q}{1-q}} \tag{8}$$

where M_0 is the threshold magnitude in the catalogue, a is a real number expressing the proportionality between the released seismic energy and the size of the fragments, and q is the entropic index from Tsallis entropy. Eq. (8) appropriately generalizes the Gutenberg–Richter relationship over a broad range of magnitudes [35] and exhibits an excellent fit to earthquake data sets [16,28,36,37]. In fact, the Gutenberg–Richter law can be easily deduced as [10,38]:

$$b = 2\cdot\frac{2-q}{q-1} \tag{9}$$

Moreover, q values obtained from different regions of the world [38] are all $q \approx 1.5-1.7$, suggesting the universality of this constant.

The aim of this study was to establish the entropy of fragments and asperities within fault fractures (i.e., within gouge fault zones) and to determine their behaviour during an earthquake. From a statistical mechanics perspective, the higher the number of microstates, the higher the entropy; and vice versa (Fig. 1).

Tsallis entropy for a continuous distribution $p(\sigma)$ of fragments of sizes σ is given by (for simplicity we set $k=1$):

$$S = \frac{1-\int_0^\infty p^q(\sigma)\,d\sigma}{q-1} \tag{10}$$

subject to two restrictions:

$$\int_0^\infty p(\sigma)\,d\sigma = 1 \tag{11}$$

and

$$\int_0^\infty \sigma p^q(\sigma)\,d\sigma = \langle\langle\sigma\rangle\rangle_q \tag{12}$$

where $\langle\langle\sigma\rangle\rangle_q$ is the mean of the distribution. Therefore, the maximum entropy principle allows us to form the following Lagrangian:

$$\mathcal{L}(p) = \frac{1-\int_0^\infty p^q(\sigma)\,d\sigma}{q-1} - \alpha\int_0^\infty p(\sigma)\,d\sigma - \beta\int_0^\infty \sigma p^q(\sigma)\,d\sigma \tag{13}$$

where α and β are the Lagrange multipliers. Imposing the Lagrangian to be extreme:

$$\frac{\partial\mathcal{L}(p)}{\partial p} = 0 \tag{14}$$

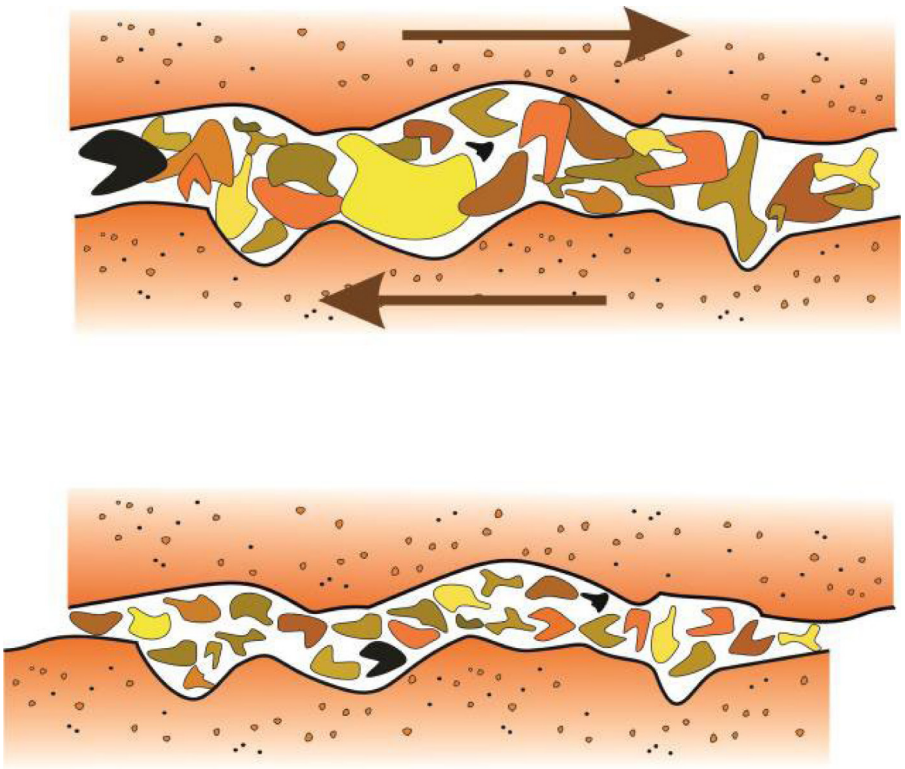

Fig. 1. Schematic visualization of the fracture contact zone before and after an earthquake. (Up) Prior to an earthquake, the state of the system, characterized by a range of fragment sizes and stress distribution forms many "microstates" compatible with fragment distribution; such entropy can be assumed to be (relatively) large. (Down) During an earthquake, fragments are broken, while asperities and barriers are overcome. Fragment sizes become homogenized and this decreases the number of possible "microstates", as such, entropy decreases. As this process is abrupt and rapid, the entropy decreases suddenly; it subsequently recovers as stress starts to re-accumulate.

it is possible to find that:

$$p(\sigma) = \frac{\left[\frac{1-q}{q}\alpha\right]^{\frac{1}{q-1}}}{[1+\beta\sigma(q-1)]^{\frac{1}{q-1}}} \tag{15}$$

where, implicitly, a cut-off condition has been used for the denominator [39,40]. If the constants A and B are defined as:

$$A \equiv \left[\frac{1-q}{q}\alpha\right]^{\frac{1}{q-1}} \tag{16}$$

and

$$B \equiv \beta(q-1) \tag{17}$$

then the size distribution function (Eq. (15)) can be rewritten as:

$$p(\sigma) = \frac{A}{[1+B\sigma]^{\frac{1}{q-1}}} \tag{18}$$

Substituting Eq. (18) into Eqs. (11) and (12), a system of equations for A and B can be obtained as follows:

$$\frac{A}{B}\frac{q-1}{2-q} = 1 \tag{19}$$

and

$$\frac{A^q}{B^2}\frac{(q-1)^2}{2-q} = 1 \tag{20}$$

for which, in this study, $1 < q < 2$ and, for simplicity, $\langle\langle\sigma\rangle\rangle_q = 1$. Hence, solving the system for A and B yields:

$$A = \left(\frac{1}{2-q}\right)^{\frac{1}{q-2}} = (2-q)^{\frac{1}{2-q}} \tag{21}$$

and

$$B = \frac{q-1}{(2-q)^{\frac{q-1}{q-2}}} = (q-1)(2-q)^{\frac{q-1}{2-q}} \tag{22}$$

From these expressions, the distribution function for fragments and asperities is:

$$p(\sigma) = \frac{(2-q)^{\frac{1}{2-q}}}{\left[1 + (q-1)(2-q)^{\frac{q-1}{2-q}}\sigma\right]^{\frac{1}{q-1}}} \tag{23}$$

Finally, by substituting Eq. (23) into that of non-extensive entropy (Eq. (10)) and solving the integral in the numerator, we can obtain:

$$S = \frac{1 - \int_0^\infty p^q(\sigma)\, d\sigma}{q-1} = \frac{1 - (2-q)^{\frac{1}{2-q}}}{q-1} \tag{24}$$

This equation allows us to find the value of the entropy for a dataset and to study its behaviour as a function of the non-extensive q parameter; therefore, if a windowing process is carried out (i.e., choosing a certain number of earthquakes and sliding the window in time), it is possible to visualize the dynamic evolution of the seismic series in terms of non-extensive entropy. The process is as follows:

1. First, the time interval W is determined for the calculation of entropy; in other words, the minimum number of earthquakes used to calculate S from Eq. (24). In general, the final window size is a reasonable compromise between the required resolution and smoothing results.
2. Second, parameter b from the Gutenberg–Richter relationship for the chosen window W is determined; this can be done from the classical expression of Aki [41] and the subsequent correction by Utsu [42]:

$$b = \frac{\log(e)}{\overline{M} - (M_0 - \frac{\Delta M}{2})} \tag{25}$$

where M_0 is the threshold magnitude; ΔM is the resolution of the magnitude (usually $\Delta M = 0.1$); and $\overline{M}$ is the average value of all possible magnitudes, which is given by:

$$\overline{M} = \int_{M_0}^{\infty} Mp(M)\, dM \tag{26}$$

The estimation of M_0 is performed using the maximum curvature (MAXC) technique [43].
3. Finally, approximation according to Sarlis et al. [38] (Eq. (9)) is used to determine q; then, the non-extensive entropy is computed for each time t following Eq. (24). By convention, the time attributed to each point of the analyses is the time of the last seismic event considered in each window.

4. Data

Variation in the relative non-extensive entropy from Eq. (24) was tested using data from earthquakes in three different tectonic environments: the 2009 M6.1 L'Aquila (Italy) earthquake, 2011 M9.0 Tohoku (Japan) megathrust earthquake, and 2016 M7.8 Kaikoura (New Zealand) earthquake. For each, we analysed several years of seismic data both before and after the mainshock.

4.1. 2009M6.1 L'Aquila (Italy) earthquake

The M6.1 L'Aquila earthquake occurred on April 6 2009, near the city of L'Aquila, in the Abruzzi region of central Italy, 100 km northeast of Rome. The earthquake resulted from normal faulting on the northwest–southeast-trending Paganica Fault [44] caused ~300 casualties, and left many more people injured and/or homeless [7]. Data were downloaded from the Istituto Nazionale di Geofisica e Vulcanologia (INGV) catalogue (http://iside.rm.ingv.it) and included 33,984 earthquakes of $M \geq 0.1$ from 2007 to 2011 (Fig. 2). The Gutenberg–Richter relationship for the dataset is shown in Fig. 3a; based on MAXC, a threshold magnitude of $M_0 = 1.5$ was chosen.

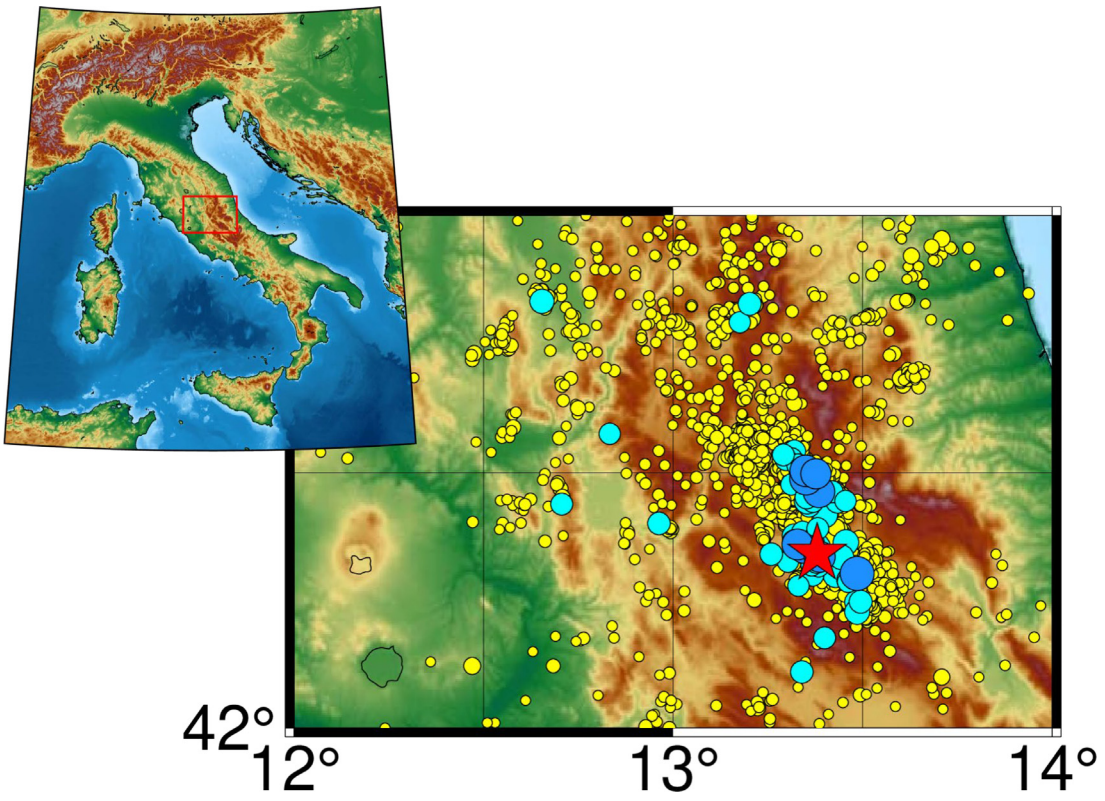

Fig. 2. Seismic activity in the Abruzzi region of central Italy from 2007 to 2011 years. The red star denotes the 2009 M6.1 L'Aquila earthquake; yellow circles are earthquakes of $2.0 \leq M \leq 3.5$ (4254 events), cyan circles are earthquakes of $3.6 \leq M \leq 4.5$ (59 events), and blue circles are earthquakes of $4.6 \leq M \leq 5.5$ (8 events).

4.2. 2011 M9.0 Tohoku (Japan) earthquake

The M9.0 Tohoku (Japan) megathrust earthquake struck on March 11 2011; it was the strongest earthquake to strike the region since record keeping began in the late 19th century. The epicentre was located ∼130 km east of the city of Sendai below the floor of the western Pacific Ocean. The earthquake was caused by a subduction zone rupture associated with the Japan Trench, which separates the Eurasian Plate from the subducting Pacific Plate [45]. The sudden horizontal and vertical thrusting of the Pacific Plate generated a huge tsunami that resulted in >15,000 casualties, the injury and displacement of thousands more, and serious damage to property and infrastructure along the coast, including the Fukushima nuclear plant [8]. Data were downloaded from the Japan Meteorological Agency (JMA) seismic catalogue (https://www.jma.go.jp), and included a total of 912,972 earthquakes in the region from 2009 to 2013 (Fig. 4). The Gutenberg–Richter relationship for the dataset is shown in Fig. 3b for a threshold magnitude of $M_0 = 1.0$.

4.3. 2016 M7.8 Kaikoura (New Zealand) earthquake

The M7.8 Kaikoura (New Zealand) earthquake struck the north-east coast of South Island, New Zealand (north of Canterbury, near the border with Marlborough) on November 13 2016; the epicentre was 60 km southwest of Kaikoura [46]. The rupture is considered one of the most complex on record [47], reflecting multiple rupturing processes along a large number of unconnected (widely spatially separated) fault segments that broke at approximately the same time. Data were downloaded from the Geo Netseismic catalogue (https://www.geonet.org.nz) and included 12,393 earthquakes in the epicentral area from 2008 to 2020 (Fig. 5). The Gutenberg–Richter relationship for the dataset is shown in Fig. 3b for a threshold magnitude of $M_0 = 2.5$.

5. Results

Fig. 6a shows magnitude versus time (in days) for earthquakes in the Abruzzi region of central Italy (2007–2011) with respect to the date of the 2009 M6.1 L'Aquila earthquake. Seismicity increased significantly after the M6.1 mainshock, and several aftershocks of M5.0–M5.5 occurred at almost the same time; the main M5.4 aftershock is highlighted in Fig. 6a.

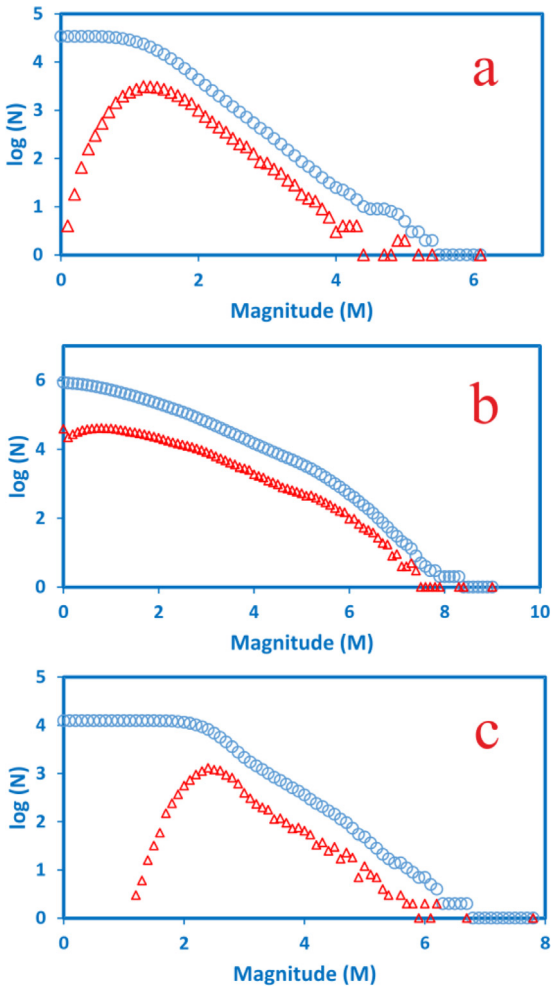

Fig. 3. Gutenberg–Richter relationships for selected earthquakes. (a) L'Aquila (2007–2011) seismicity, (b) Tohoku (2009–2013) seismicity, and (c) Kaikoura (2008–2016) seismicity. The threshold magnitudes (M_0) were 1.5, 1.0, and 2.5 for the data in (a), (b), and (c), respectively.

Fig. 6b shows non-extensive entropy S resulting from the windowing process (using Eq. (24)) applied to the seismic sequence. An abrupt decrease in the relative value of the non-extensive entropy S is coincident with the mainshock; values then recovered to a level similar to that prior to the mainshock. Smaller decreases followed subsequent earthquakes, including a M4.4 event on June 22 2009 (77 days after the mainshock) and a M4.1 even on August 28 2010 (509 days after the mainshock).

Fig. 7a shows magnitude versus time (in days) for earthquakes in the Tohoku region of Japan (2009–2013) with respect to the date of the 2011 M9.0 Tohoku (Japan) earthquake, including four significant subsequent earthquakes with magnitudes ranging from M7.3 to M6.9. Fig. 7b shows non-extensive entropy S resulting from the windowing process (using Eq. (24)) applied to the seismic sequence. An abrupt decrease in non-extensive entropy S was coincident with the mainshock, after which values partially recovered. Full recovery of non-extensive entropy S values was likely prevented by the numerous major aftershocks in the hours after the mainshock; in the first 3 h following the mainshock, 16 aftershocks with magnitudes of > 6.5 occurred (three of them $>$ M7). Further abrupt decreases occurred following major aftershocks at 120, 360, 630, and 960 days after the mainshock.

Fig. 8a shows magnitude versus time (in days) for earthquakes in the northern Canterbury region of New Zealand (2008–2020) with respect to the date of the 2016 M7.8 Kaikoura earthquake (November 13 2016). Fig. 8b shows non-extensive entropy S resulting from the windowing process (using Eq. (24)) applied to the seismic sequence. Seismicity in the epicentral area was low prior to the mainshock; in the 8 years before the Kaikoura earthquake, only $\sim$1300 earthquakes of $>$M2.5 were recorded, among which only a M6.2 on April 24 2015, was significant. Numerous aftershocks occurred in the hours following the M7.8 Kaikoura mainshock (M5.8–M6.7, with at least four events of $>$M6.0). After the mainshock, seismicity remained elevated for a few months, after which it declined again. A moderate M5.6 earthquake occurred in the area 1 year after the mainshock. Non-extensive entropy S was very stable until the M7.8 Kaikoura

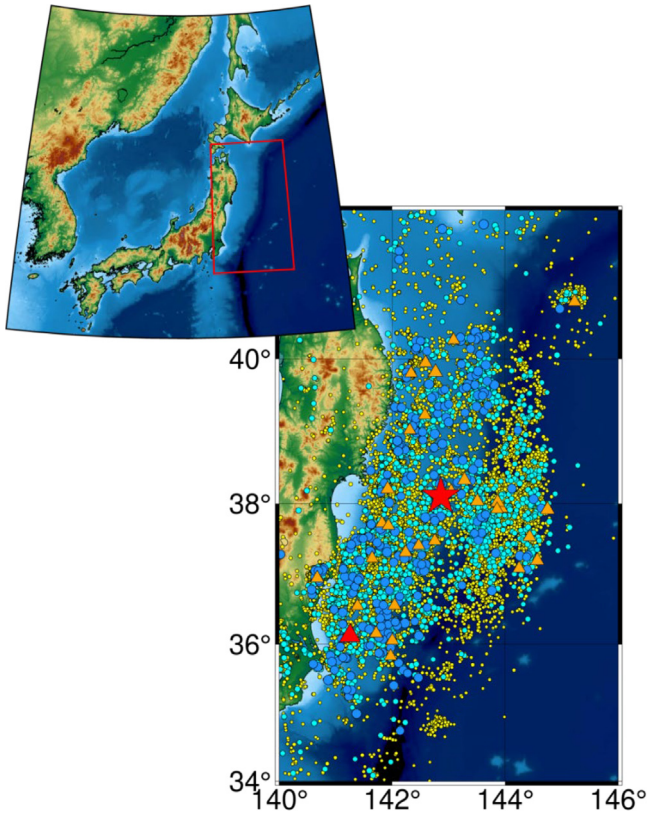

Fig. 4. Seismicity in the Tohoku region of Japan from 2009 to 2013. The red star denotes the 2011 M9.0 Tohoku earthquake, located ∼130 km east of the city of Sendai, Miyagi Prefecture, in the Pacific Ocean. Yellow circles denote earthquakes of $3.5 \leq M \leq 4.5$ (15,637 events), cyan circles denote earthquakes of $4.6 \leq M \leq 5.5$ (1853 events), blue circles denote earthquakes of $5.6 \leq M \leq 6.5$ (259 events), orange triangles denote earthquakes of $6.6 \leq M \leq 7.5$ (30 events), and the red triangle denotes an M7.6 aftershock on March 3 2011.

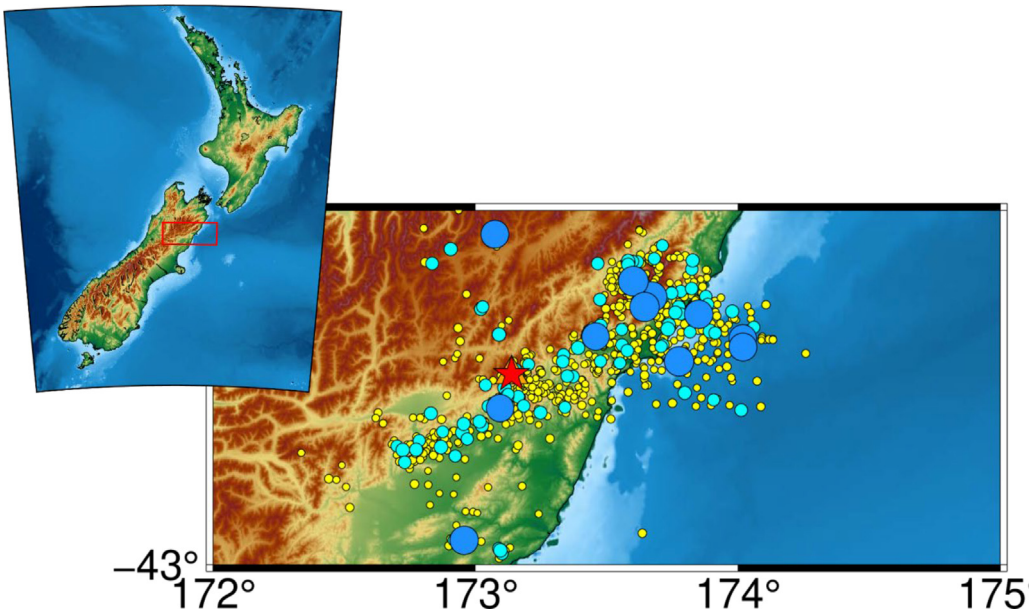

Fig. 5. Seismicity in the northern Canterbury region of New Zealand from 2008 to 2020. The red star denotes the 2016 M7.8 Kaikoura earthquake; yellow circles denote earthquakes of $3.5 \leq M \leq 4.5$ (632 events), cyan circles denote earthquakes of $4.6 \leq M \leq 5.5$ (92 events), blue circles denote earthquakes of $5.6 \leq M \leq 6.5$ (11 events), and the orange triangle is a M6.7 aftershock on November 14 2016.

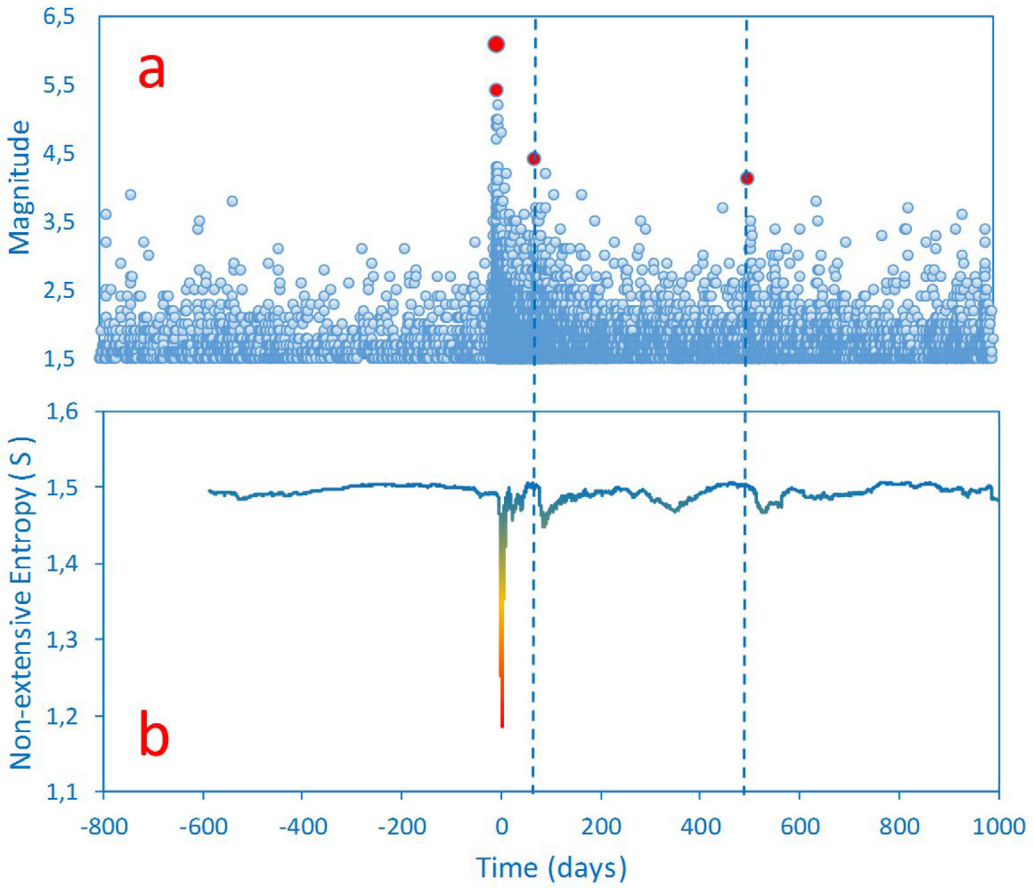

Fig. 6. Regional seismicity (2007–2011) and non-extensive entropy (*S*) associated with the 2009 M6.1 L'Aquila earthquake. (a) Magnitude versus time with respect to the mainshock (on April 62009), shown by the large red circle. The main aftershocks are shown by smaller red circles and include a M5.4 on April 6 2009, M4.4 on June 22, 2009 (77 days after the mainshock), and M4.1 on August 28, 2010 (509 days after the mainshock). (b) Non-extensive entropy (*S*). Dashed lines mark slight decreases in entropy coincident with the times of major aftershocks.

mainshock, at which point it decreased abruptly and then recovered, indicating a return to the "metastability" of the system. An M6.2 earthquake on April 24, 2015 (2 years before the mainshock) and a M5.6 aftershock on October 22 2017, both caused more limited decreases in entropy values.

6. Conclusions

In this study, we applied a fragment–asperity interaction model [28] to seismic data on order to obtain a mathematical expression of the non-extensive entropy (S) of fragments and asperities (see Eq. (24)) in the gouge area based on Tsallis entropy. We were able to derive entropy values for earthquake catalogues depending on the q non-extensive parameter. Moreover, we developed a methodology to identify the occurrence of earthquakes from the dynamic evolution of non-extensive entropy. This approach includes: (1) definition of a windowing process, (2) computation of the b value for each window following Utsu [40] and the MAXC technique [41], (3) estimation of the q non-extensive parameter following Sarlis et al. [38], and (4) the calculation of non-extensive entropy. Based on analysis of three earthquake sequences (the 2009 M6.1 L'Aquila earthquake, 2011 M9.0 Tohoku megathrust earthquake, and 2016 M7.8 Kaikoura earthquake), our results show that S offers an indicator of the equilibrium state of seismically active regions. Sudden changes in non-extensive entropy are associated with earthquakes. Moreover, it is also possible to detect earthquakes considered as aftershocks or those that are subsequent to a previous event in another part of the seismic system but that would not have occurred without the mainshock (i.e., triggered earthquakes).

We would like to emphasize that Eq. (24) incorporates the characteristics of non-extensivity into the distribution of earthquakes entropy and illustrates an important relationship between entropy and the non-extensive parameter q.

Most previous works that have used the original fragment–asperity interaction model [28], or with the improve version [29,32,33], have concluded that maximum of the entropy occurs at $q \approx 1.6$. Fig. 9 shows a graphical representation

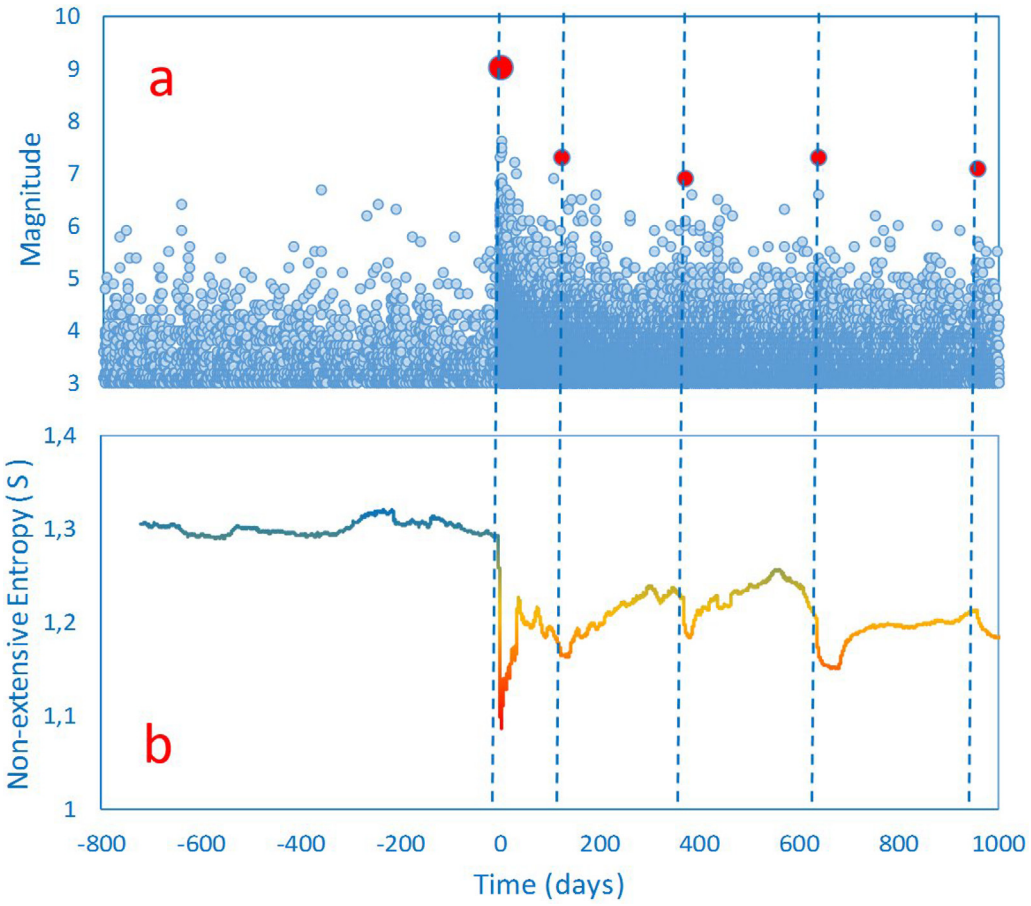

Fig. 7. Regional seismicity (2009–2013) and non-extensive entropy (*S*) associated with the 2011 M9.0 Tohoku megathrust earthquake. (a) Magnitude versus time with respect to the mainshock (on March 11 2011), shown by the large red circle. The main aftershocks are shown by smaller red circles and include a M7.3 on July 10 2011, M6.9 on March 14 2012, M7.3 on 7 December 2012 (December 7), and M7.1 on October 26 2013. (b) Non-extensive entropy (*S*). Dashed lines mark decreases in entropy coincident with the times of the mainshock and major aftershocks.

of Eq. (24), as obtained in this study, and explicitly illustrates how this new theoretical result definitively fits the empirical applications obtained in different seismically active regions of the world.

Eq. (24) offers a method to identify entropy as a function of the not-extensive parameter q, but also as a function of seismic magnitude. Indeed, the relationship between geometry (size) of fragments and asperities in the fracture region and the relaxed seismic energy and, therefore, the magnitude of the earthquake make it possible to identify strong dependence between entropy and the parameters q and M.

Finally, through this work, we have illustrated the exportability of some classical concepts of thermodynamics and statistical physics, such as entropy and the second law, to others scientific fields, including the study of non-linear phenomena (e.g., earthquakes).

Declaration of competing interest

The authors declare that they have no known competing financial interests or personal relationships that could have appeared to influence the work reported in this paper.

Data availability

Data will be made available on request.

Acknowledgements

The authors are grateful to INGV (Italy), JMA (Japan), and GeoNet (New Zealand) for providing the data used in this work. This work was partially supported by the RNM194 research group of Junta de Andalucía (Spain). English language editing was performed by Tornillo Scientific.

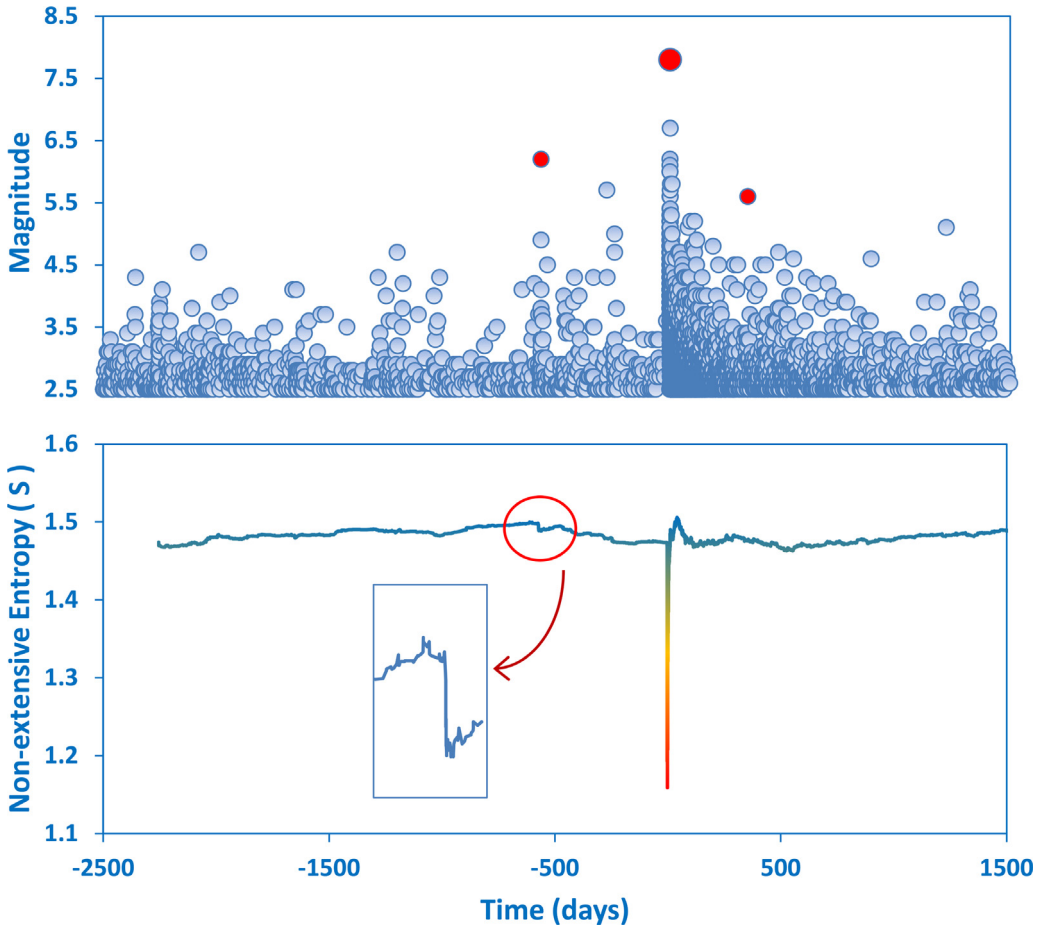

Fig. 8. Regional seismicity (2008–2020) and non-extensive entropy (*S*) associated with the 2016 M7.8 Kaikoura earthquake. (a) Magnitude versus time with respect to the mainshock (on November 13 2016), shown by the large red circle. Smaller red circles denote a M6.2 earthquake on April 24 2015 (2 years before the mainshock) and a M5.6 aftershock on October 22 2017. (b) Non-extensive entropy (*S*). The box shows a zoomed in view of *S* before and after the 2015 foreshock.

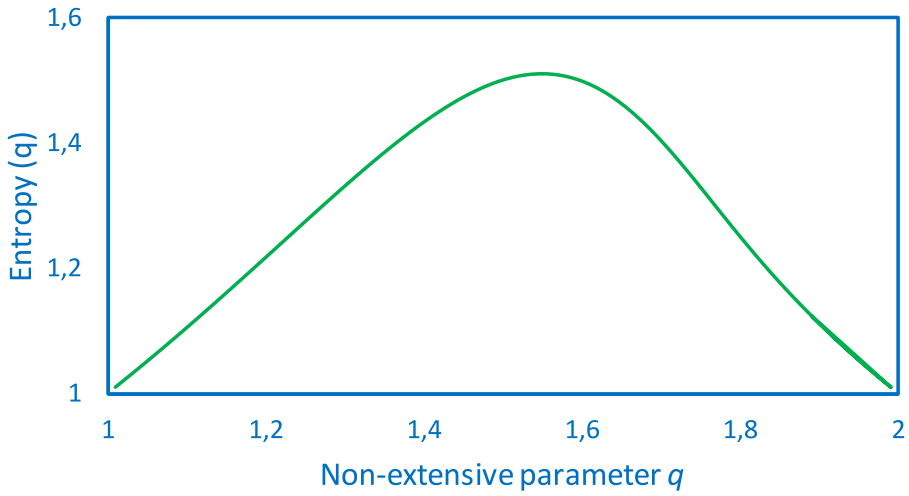

Fig. 9. Graphical representation of the non-extensive entropy function (Eq. (24)). Maximum entropy is at $q \approx 1.6$ which agrees with previous studies in other seismic zones around the world.

References

[1] Ben-Naim A. Entropy, Shannon's measure of information and Boltzmann's H-theorem. Entropy 2017;19:48. http://dx.doi.org/10.3390/e19020048.
[2] Akopian STs. Seismic systems of Japan: Entropy and monitoring of the tohoku earthquake. SeisInstrum 2014;50(4):347–68. http://dx.doi.org/10.3103/S0747923914040021, 2011.
[3] Billio M, Casarin R, Costola M, Pasqualini A. An entropy based early warning indicator for systemic risk, vol. 12. SYRTO working paper series, 2015.
[4] Vallianatos F, Michas G, Papadakis, G. Nonextensive statistical seismology: An overview. In: Chelidze T, Vallianatos F, Telesca L, editors. Complexity of seismic time series. Complexity of seismic time series: Measurement and application, Elsevier; 2018, p. 25–59. http://dx.doi.org/10.1016/B978-0-12-813138-1.00002-X.
[5] Tsallis C. Nonextensive statistical mechanics and thermodynamics: historical background and present status. In: Abe S, Okamoto Y, editors. Nonextensive statistical mechanics and its applications, vol. 560. Lecture notes in physics, Berlin-Heildelberg: Springer; 2001, p. 398.
[6] Telesca L, Lapenna V, Lovallo M. Information entropy analysis of seismicity of Umbria Marché region (central Italy). Nat Hazard Earth SystSci 2004;4:691–5. http://dx.doi.org/10.5194/nhess-4-691-2004.
[7] De Santis A, Cianchini G, Favali P, Beranzoli L, Boschi E. The Gutenberg–Richter law and entropy of earthquakes: two case studies in central Italy. Bull Seismol Soc Am 2001;101:1386–95. http://dx.doi.org/10.1785/0120090390.
[8] Sarlis NV, Skordas ES, Varotsos PA. A remarkable change of the entropy of seismicity in natural time under time reversal before the super-giant m9 tohoku earthquake on 11 2011. EPL2018, vol. 124, p. 29001. http://dx.doi.org/10.1209/0295-5075/124/29001.
[9] Varotsos PA, Skordas ES, Sarlis NV. Fluctuations of the entropy change under time reversal: Further investigations on identifying the occurrence time of an impending major earthquake. EPL2020, vol. 130, p. 29001. http://dx.doi.org/10.1209/0295-5075/130/29001.
[10] Telesca L. Analysis of Italian seismicity by using a nonextensive approach. Tectonophysics 2010a;494:155–62. http://dx.doi.org/10.1016/j.tecto.2010.09.012.
[11] Telesca L. Nonextensive analysis of seismic sequences. Phys A 2010b;389:1911–4. http://dx.doi.org/10.1016/j.physa.2010.01.012.
[12] Telesca L. A non-extensive approach in investigating the seismicity of L' Aquila area (central Italy) struck by the 6 2009 earthquake (ML5.8). Terra Nova 2010c;22(2):87–93. http://dx.doi.org/10.1111/j.1365-3121.2009.00920.x.
[13] Valverde-Esparza SM, Ramírez-Rojas A, Flores-Márquez EL, Telesca L. Non-extensivity analysis of seismicity within Four Subduction Regions in Mexico. Acta Geophys 2012;60(3):833–45. http://dx.doi.org/10.2478/s11600-012-0012-1.
[14] Michas G, Vallianatos F, Sammonds P. Non-extensivity and long-range correlations in the earthquake activity at the west corinth rift (Greece). Nonlinear Process Geophys 2013;20:713–24. http://dx.doi.org/10.5194/npg-20-713-2013.
[15] Papadakis G, Vallianatos F, Sammonds P. A nonextensive statistical physics analysis of the 1995 kobe, Japan earthquake. Pure ApplGeophys 2015;172:1923–31. http://dx.doi.org/10.1007/s00024-014-0876-x.
[16] Varotsos PA, Sarlis NV, Skordas ES. Tsallis entropy index q and the complexity measure of seismicity in natural time under time reversal before the M9 tohoku earthquake in 2011. Entropy 2018;20:757–73. http://dx.doi.org/10.3390/e20100757.
[17] Skordas ES, Sarlis NV, Varotsos PA. Precursory variations of Tsallis non-extensive statistical mechanics entropic index associated with the M9 Tohoku earthquake in 2011. EurPhys J Special Topics 2020;229:851–9. http://dx.doi.org/10.1140/epjst/e2020-900218-x.
[18] Zupanovic P, Domagoj K. Relation between Boltzmann and Gibbs entropy and example with multinomial distribution. J PhysCommun 2018;2:045002. http://dx.doi.org/10.1088/2399-6528/aab7e1.
[19] Shannon CE. A mathematical theory of communication. Bell Sys Tech 1948;27:379423.
[20] Shannon CE, Weaver W. The mathematical theory of communication. The Board of Trustees of the University of Illinois; 1949.
[21] Tsallis C. Possible generalization of Boltzmann–Gibbs statistics. J Stat Phys 1988;52:479487. http://dx.doi.org/10.1007/BF01016429.
[22] Vallianatos F, Papadakis G, Michas G. Generalized statistical mechanics approaches to earthquakes and tectonics. Proc R Soc Lond Ser A Math Phys Eng Sci 2016;472:20160497. http://dx.doi.org/10.1098/rspa.2016.0497.
[23] Tsallis C. Introduction to nonextensive statistical mechanics: Approaching a complex world. Berlin: Springer; 2009, http://dx.doi.org/10.1007/978-0-387-85359-8.
[24] Posadas A, Morales J, Ibañez JM, Posadas-Garzon A. Shaking earth: Non-linear seismic processes and the second law of thermodynamics: A case study from Canterbury (New Zealand) earthquakes. Chaos, Solitons Fract 2021;151. http://dx.doi.org/10.1016/j.chaos.2021.111243.
[25] Berrill JB, Davis RO. Maximum entropy and the magnitude distribution. Bull Seismol Soc Am 1980;70:1823–31.
[26] Shen PY, Mansinha L. On the principle of maximum entropy and the earthquake frequency–magnitude relation. Geophys J R Astr Soc 1983;74:777–85. http://dx.doi.org/10.1111/j.1365-246X.1983.tb01903.x.
[27] Main I, Burton PW. Information theory and the earthquake frequency–magnitude distribution. Bull Seismol Soc Am 1984;74:1409–26. http://dx.doi.org/10.1785/BSSA0740041409.
[28] Sotolongo-Costa O, Posadas A. Fragment–asperity interaction model for earthquakes. Phys Rev Lett 2004;92(4):048501. http://dx.doi.org/10.1103/PhysRevLett.92.048501.
[29] Silva R, Franca GS, Vilar CS, Alcaniz JS. Nonextensive models for earthquakes. Phys Rev E 2006;7:026102. http://dx.doi.org/10.1103/PhysRevE.73.026102.
[30] Lay T, Wallace T. Modern global seismology. New York: Academic Press; 1995.
[31] Darooneh A, Mehri A. A nonextensive modification of the Gutenberg–Richter law: q-stretched exponential form. Physica A 2010;389:509–14. http://dx.doi.org/10.1016/j.physa.2009.10.006.
[32] Telesca L. Tsallis-based nonextensive analysis of the southern California seismicity. Entropy 2011;13(7):1267–80. http://dx.doi.org/10.3390/e13071267.
[33] Telesca L. Maximum likelihood estimation of the nonextensive parameters of the earthquake cumulative magnitude distribution. Bull Seismol Soc Am 2012;102(2):886–91. http://dx.doi.org/10.1785/0120110093.
[34] Kanamori H. Quantification of earthquakes. Nature 1978;271:411–4.
[35] Vallianatos F, Michas G, Papadakis G. A description of seismicity based on non-extensive statistical physics: a review. In: D'Amico S, editor. Earthquakes and their impact on society. Cham: Springer Natural Hazards; 2015, p. 1–41. http://dx.doi.org/10.1007/978-3-319-21753-6.
[36] Vilar CS, Franca GS, Silva R, Alcaniz JS. Nonextensivity in geological faults? Phys A 2007;377:285–90. http://dx.doi.org/10.1016/j.physa.2006.11.017.
[37] Michas G. Generalized statistical mechanics description of fault and earthquake populations in corinth rift (greece) (Ph.D. thesis), University College London; 2016.
[38] Sarlis NV, Skordas ES, Varotsos PA. Nonextensivity and natural time: The case of seismicity. Phys Rev E 2010;82:021110. http://dx.doi.org/10.1103/PhysRevE.82.021110.
[39] Khordad R, Rastegar Sedehi HR, Sharifzadeh M. Susceptibility, entropy and specific heat of quantum rings in monolayer graphene: comparison between different entropy formalisms. J Comput Electr 2022;21:422–30. http://dx.doi.org/10.1007/s10825-022-01857-1.

[40] Rastegar Sedehi HR, Bazrafshan A, Khordad R. Thermal properties of quantum rings in monolayer and bilayer graphene. Solid State Commun 2022;353:114853. http://dx.doi.org/10.1016/j.ssc.2022.114853.
[41] Aki K. Maximum likelihood estimate of b in the formula log (N)=a-bm and its confidence limits. Bull Earthq Res Inst Tokyo Univ 1965;43:237–9.
[42] Utsu T. A method for determining the value of b in a formula log n=a–bm showing the magnitude-frequency relation for earthquakes. Geophys Bull Hokkaido Univ 1965;13:99–103.
[43] Wiemer S, Wyss M. Minimum magnitude of complete reporting in earthquake catalogs: examples from Alaska, the Western United States, and Japan. Bull Seismol Soc Am 2000;90:859–69. http://dx.doi.org/10.1785/0119990114.
[44] Falcucci E, Gori S, Peronace E, Fubelli G, Moro M, Saroli M, Giaccio B, Messina P, Naso G, Scardia G, Sposato A, Voltaggio M, Galli P, Galadini F. The paganica fault and surface coseismic ruptures caused by the 6 2009 earthquake (L'aquila, central Italy). Seismol. Res Lett 2009;80(6):940–50. http://dx.doi.org/10.1785/gssrl.80.6.940.
[45] Fujii Y, Satak K, Sakai S, Shinohara M, Kanazawa T. Tsunami source of the 2011 off the Pacific coast of Tohoku Earthquake. Earth Planet Sp 2011;63:55. http://dx.doi.org/10.5047/eps.2011.06.010.
[46] Hollingsworth J, Ye L, Avouac P. Dynamically triggered slip on a splay fault in the Mw 7.8, 2016 kaikoura (New Zealand) earthquake. Geophys Res Lett 2017;44:3517–25. http://dx.doi.org/10.1002/2016GL072228.
[47] Cesca S, Zhang, Mouslopoulou V, Wang R, Saul J, Savage M, Heimann S, Kufner SK, Oncken O, Dahm T. Complex rupture process of the Mw 7.8, 2016, kaikoura earthquake, New Zealand, and its aftershock sequence. Earth Sci Lett 2017;478:110–20. http://dx.doi.org/10.1016/j.epsl.2017.08.024.